

Local and intrinsic quantum coherence in critical systemsSu-Peng Li¹ and Zheng-Hang Sun^{2,3,*}¹*Department of Physics, Huazhong Normal University, Wuhan, Hubei 430079, China*²*Institute of Physics, Chinese Academy of Sciences, Beijing 100190, China*³*School of Physical Sciences, University of Chinese Academy of Sciences, Beijing 100190, China*

(Received 2 June 2018; published 14 August 2018)

Local and intrinsic quantum coherence, as two contributions of total quantum coherence, have been introduced by Radhakrishnan *et al.* [C. Radhakrishnan, M. Parthasarathy, S. Jambulingam, and T. Byrnes, *Phys. Rev. Lett.* **116**, 150504 (2016)]. In the present work we study the property of local, intrinsic, and total quantum coherence in critical systems such as the XY model, extended XY model, and Ashkin-Teller model to analyze their capability in identifying the second-order, infinite-order quantum phase transitions, as well as the topological quantum phase transitions. It is shown that not only the total coherence, but also the local and intrinsic coherence can spotlight the critical points efficiently. Moreover, the long-range properties of total and local coherence, and the short-range properties of intrinsic coherence are analyzed. The total and local coherence for spin-pairs farther than nearest neighbors can highlight the critical points while the intrinsic coherence is absent for long-distance spin-pairs.

DOI: [10.1103/PhysRevA.98.022317](https://doi.org/10.1103/PhysRevA.98.022317)**I. INTRODUCTION**

Quantum coherence plays a crucial role in quantum information science and is regarded as an important resource in various quantum information tasks [1,2]. The theoretical framework for the quantification of quantum coherence is rigorously introduced by Baumgratz, Cramer, and Plenio [3], where the relative entropy and the l_1 norm are proved to be proper distance measures for quantifying quantum coherence. Several remarkable efforts have been devoted to exploring quantum coherence over the past few years. For instance, the measures of quantum coherence based on the Tsallis relative α entropies [4], trace-norm distance [5,6], fidelity [6], and skew information [7,8] are fully studied. Additionally, the distribution of quantum coherence was first introduced by Radhakrishnan *et al.*, in which the total quantum coherence was decomposed into the intrinsic coherence and the local coherence that can be interpreted as the collective coherence between two subsystems and the coherence on every single subsystem, respectively [9].

It is well known that the quantum phase transitions (QPTs), which are induced by quantum fluctuation, are one of the central topics in condensed-matter physics [10]. Recently, the relation between quantum coherence and QPTs has attracted great attention and it has been shown that the derivative of quantum coherence quantified by the relative entropy [11], quantum Jensen-Shannon divergence [12], l_1 norm [13], and skew information [13,14] can be efficient probes of the second-order QPT in the XY model. It is now recognized that most of the previous works only investigated the total quantum coherence in critical systems. Moreover, although Radhakrishnan *et al.* studied the total, local, and intrinsic quantum coherence in XXZ spin-1/2 chain and indicated

that all of them can characterize the first-order QPT in this model [9], the local and intrinsic quantum coherence in critical systems where the second-order QPTs, infinite-order QPTs, and topological quantum phase transitions (TQPTs) occur, were not investigated carefully.

In contrast to the first, second, and infinite-order QPTs, which are characterized by the Landau-Ginzburg-Wilson paradigm [10], TQPTs are beyond the symmetry-breaking theory of Landau and can be described by nonlocal string order parameters [15,16]. In this work, we focus on the extended XY model, where the three-body interaction is considered. The extended XY spin-1/2 chain is an integrable model with rich quantum phases, including the paramagnetic phase and the ferromagnetic phase in XY model when the three-site interaction is neglected and several topological phases characterized by different winding numbers because of the \mathbb{Z} symmetry [17]. Consequently, it can be regarded as an ideal platform to demonstrate the capability of local and intrinsic quantum coherence in identifying the second-order QPTs and TQPTs.

Furthermore, to investigate the relation between quantum coherence and infinite-order QPT, we will study the local and intrinsic quantum coherence in the Ashkin-Teller (A-T) model [18], which can be experimentally realized on Ni(100) surface with absorbed selenium [19]. The infinite-order QPT in the A-T model has been characterized via the extreme points of the entanglement entropy for a block subsystem [20] and the global quantum discord [21]. Nevertheless, the signature of the infinite-order QPT can not be detected by the pairwise entanglement straightforwardly [20].

The primary motivation of the present work is to explore whether the total, local, and intrinsic quantum coherence can be indicators of TQPTs, second and infinite-order QPTs or not. Towards that goal, the behaviors of total, local, and intrinsic quantum coherence near the critical points associated to the second-order QPT in the XY model, the TQPTs in the extended XY model, and the infinite-order QPT in the

*zhenghangsun@outlook.com

A-T model are studied carefully. Both of the total and local quantum coherence can characterize the second-order QPT and TQPTs for the long-distance spin-pairs of the XY model and the extended XY model, respectively. Whereas, the intrinsic coherence can only spotlight the critical points for the spin-pairs with short distance of the spin chains. The two-site scaling laws are obtained by analyzing the long-distance properties of total quantum coherence. Additionally, we prove that there is no intrinsic coherence for the frontal spin-pairs of the A-T spin chain. Therefore, the local coherence becomes the main contribution of total quantum coherence. It is nontrivial that the local coherence, which is equal to the total coherence, can detect the infinite critical point in A-T model efficiently.

The remainder of this work is organized as follows. In Sec. II, first, the extended XY model and the A-T model are briefly reviewed. Second, the definition of total, intrinsic, and local quantum coherence are given. In Sec. III, the calculation results of total, intrinsic, and local quantum coherence in the XY model, extended XY model, and A-T model are presented. In Sec. IV we conclude.

II. MODELS AND DEFINITIONS

A. Extended XY model

The Hamiltonian of the extended XY model can be written as [17]

$$H = \sum_{i=1}^N \alpha \sigma_i^z \left(\frac{1+\delta}{2} \sigma_{i-1}^x \sigma_{i+1}^x + \frac{1-\delta}{2} \sigma_{i-1}^y \sigma_{i+1}^y \right) + \sum_{i=1}^N \left(\frac{1+\gamma}{2} \sigma_i^x \sigma_{i+1}^x + \frac{1-\gamma}{2} \sigma_i^y \sigma_{i+1}^y + \lambda \sigma_i^z \right), \quad (1)$$

where γ and δ denote the anisotropy of the spin chain, α represents the strength of three-site interaction, and λ is the strength of the magnetic field. The Pauli operators in Eq. (1) can be mapped to spinless fermion operators by applying the Jordan-Wigner transformation. Then, after the Fourier-Bogoliubov transformation, in momentum space, the Hamiltonian can be diagonalized as [22–24]

$$H = \sum_k \varepsilon_k \left(\eta_k^\dagger \eta_k - \frac{1}{2} \right), \quad (2)$$

where $k = \frac{2\pi M}{N}$ and $M = -\frac{N-1}{2}, -\frac{N-3}{2}, \dots, \frac{N-3}{2}, \frac{N-1}{2}$. The relation between the Bogoliubov fermion operator η_k and the fermionic operators in momentum space c_k is $c_k = \cos \frac{\theta_k}{2} \eta_k + i \sin \frac{\theta_k}{2} \eta_{-k}^\dagger$ with

$$\tan(\theta_k) = \frac{Y(k)}{Z(k)}, \quad (3)$$

where $Y(k) = \alpha \delta \sin(2k) + \gamma \sin k$ and $Z(k) = \alpha \cos(2k) + \cos k - \lambda$, and the energy spectra read $\varepsilon_k = \pm \sqrt{Y^2(k) + Z^2(k)}$.

The reduced density operator for the spin-pair consisted of m th and n th spin can be written as

$$\rho_{mn} = \frac{1}{4} \begin{pmatrix} w^+ & 0 & 0 & v^- \\ 0 & z & v^+ & 0 \\ 0 & v^+ & z & 0 \\ v^- & 0 & 0 & w^- \end{pmatrix}, \quad (4)$$

where $w^\pm = 1 \pm 2\langle \sigma^z \rangle + \langle \sigma_m^z \sigma_n^z \rangle$, $z = 1 - \langle \sigma_m^z \sigma_n^z \rangle$, and $v^\pm = \langle \sigma_m^x \sigma_n^x \rangle \pm \langle \sigma_m^y \sigma_n^y \rangle$. The correlation functions read

$$\langle \sigma^z \rangle = -G_0, \quad (5)$$

$$\langle \sigma_m^z \sigma_n^z \rangle = G_0^2 - G_R G_{-R}, \quad (6)$$

$$\langle \sigma_m^x \sigma_n^x \rangle = \begin{vmatrix} G_{-1} & G_{-2} & \cdots & G_{-R} \\ G_0 & G_{-1} & \cdots & G_{-R+1} \\ \vdots & \vdots & \ddots & \vdots \\ G_{R-2} & G_{R-3} & \cdots & G_{-1} \end{vmatrix}, \quad (7)$$

$$\langle \sigma_m^y \sigma_n^y \rangle = \begin{vmatrix} G_1 & G_0 & \cdots & G_{-R+2} \\ G_2 & G_1 & \cdots & G_{-R+3} \\ \vdots & \vdots & \ddots & \vdots \\ G_R & G_{R-1} & \cdots & G_1 \end{vmatrix}, \quad (8)$$

where $R = |m - n|$ is the distance of spin-pairs, and $G_R = -\frac{1}{\pi} \int_0^\pi dk \cos(Rk - \theta_k)$ in the case of zero temperature.

The Hamiltonian (1) becomes the XY model in the case of $\alpha = 0$. There is a second-order QPT between the paramagnetic phase and ferromagnetic phase at the critical point $\lambda_c = 1$. Moreover, it is worth mentioning that the factorization phenomenon also exists in the XY model and the factorization points satisfy $\lambda_f = \sqrt{1 - \gamma^2}$ [13,14,25].

Next we analyze the TQPTs in the extended XY model. Actually, in momentum space, the Hamiltonian (1) can be expressed as the form of the Bogoliubov–de Gennes Hamiltonian

$$H = \sum_k \begin{pmatrix} c_k^\dagger & c_{-k} \end{pmatrix} \mathcal{H}_k \begin{pmatrix} c_k \\ c_{-k}^\dagger \end{pmatrix}, \quad (9)$$

where $\mathcal{H}_k = \vec{r}(k) \cdot \vec{\sigma}$ with $\vec{r}(k) = (0 \quad Y(k) \quad Z(k))$. In the auxiliary Y – Z plane, the winding number with respect to the origin point reads

$$\nu = \frac{1}{2\pi} \oint (YdZ - ZdY) / |\vec{r}|^2. \quad (10)$$

The critical points of TQPTs can be obtained by solving the characteristic equation $g(\xi) = 0$, where $g(\xi) = \alpha[\xi^2 + (1 - \delta)\xi^{-2}/2] + \xi + (1 - \gamma)\xi^{-1}/2 - \lambda$, and $\xi = \exp(ik)$, with $|\xi| = 1$. For example, with the parameters $\alpha = 1$, $\delta = 1$, and $\lambda = -0.5$, it can be numerically verified that $\gamma_{c1} \simeq -0.618$ and $\gamma_{c2} \simeq 1.618$ satisfy the characteristic function. Moreover, the energy spectra displayed in Fig. 1(a) also indicate that $\gamma_{c1} \simeq -0.618$ and $\gamma_{c2} \simeq 1.618$ are the critical points of TQPTs. The winding numbers can be directly obtained from the trajectories of winding vectors in the auxiliary Y – Z plane. The trajectories for $\gamma = -1, 0, 2$ are presented in Fig. 1(b), which suggest that with the increase of γ , the winding number ν changes from 0 to 2 at γ_{c1} and from 2 to 0 at γ_{c2} .

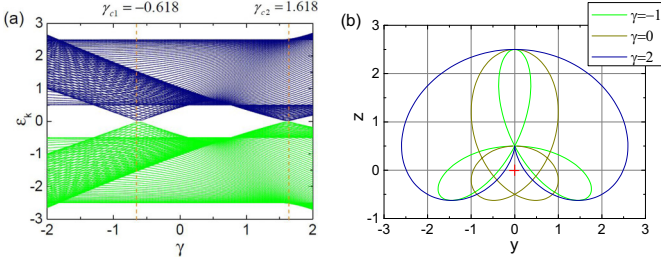


FIG. 1. (a) The energy spectra as a function of γ with parameters $\alpha = 1$, $\delta = 1$, and $\lambda = -0.5$. (b) Trajectories of winding vectors in Y - Z plane with parameters $\alpha = 1$, $\delta = 1$, $\lambda = -0.5$, and $\gamma = -1, 0, 2$.

B. Ashkin-Teller model

The Hamiltonian of the Ashkin-Teller (A-T) model is given as

$$H_{AT} = - \sum_{i=1}^M (\sigma_i^x + \tau_i^x + \Delta \sigma_i^x \tau_i^x) - \beta \sum_{i=1}^M (\sigma_i^z \sigma_{i+1}^z + \tau_i^z \tau_{i+1}^z + \Delta \sigma_i^z \sigma_{i+1}^z \tau_i^z \tau_{i+1}^z), \quad (11)$$

where σ_i^η and τ_i^η ($\eta = x, y, z$) represent independent Pauli operators. M is the length of the A-T spin chain with $N = 2M$ spins. The location of the critical point related to infinite-order QPT is $\Delta_c = 1$, which is irrelevant to the value of β . Here we adopt the periodic boundary condition, that is, $\sigma_{M+1}^\eta = \sigma_1^\eta$ and $\tau_{M+1}^\eta = \tau_1^\eta$.

The scheme of the A-T model is shown in Fig. 2. Here, we focus on the frontal spin-pairs at the i th site, which is marked by the red circle in Fig. 2. The reduced density matrix for the i th frontal spin-pairs can be written as [20]

$$\rho_{\sigma_i - \tau_i} = \frac{1}{4} \begin{pmatrix} 1 & u & u & v \\ u & 1 & v & u \\ u & v & 1 & u \\ v & u & u & 1 \end{pmatrix}, \quad (12)$$

where $u = \langle \sigma_i^x \rangle = \langle \tau_i^x \rangle$ and $v = \langle \sigma_i^x \tau_i^x \rangle$.

C. Total, local, and intrinsic quantum coherence

The general form of total quantum coherence can be written as [1–3]

$$\mathcal{C}_T(\rho) = \min_{\delta \in \mathcal{I}} \mathcal{D}(\rho, \delta), \quad (13)$$

where \mathcal{D} is a distance measure and \mathcal{I} denotes a set of incoherent states. A proper distance measure \mathcal{D} for quantifying quantum coherence should satisfy several conditions as proposed by the

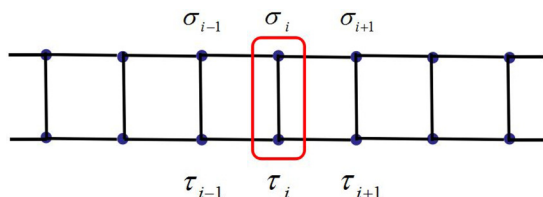


FIG. 2. The scheme of Ashkin-Teller model.

authors of Ref. [3]. The total quantum coherence (13) can be divided into the coherence *between* different subsystems and the coherence *on* every single subsystem, which are named as the intrinsic coherence and the local coherence, respectively [9].

It is worth stressing that the total quantum coherence is dependent on the chosen basis because ρ is an incoherent state in the basis consisted of the eigenstates of ρ . In Ref. [9], the intrinsic quantum coherence, which is a basis-independent quantity, is defined as

$$\mathcal{C}_I(\rho) = \min_{\delta \in \mathcal{S}} \mathcal{D}(\rho, \delta), \quad (14)$$

where \mathcal{S} represents a set of separable states. In fact, the intrinsic coherence is equal to the quantum entanglement measured via distance \mathcal{D} [26]. In addition, incoherent states are diagonal in a chosen orthogonal basis, which are definitely separable; nevertheless separable states are not necessarily incoherent. Therefore the relation between two sets \mathcal{I} and \mathcal{S} clearly appears as $\mathcal{I} \subset \mathcal{S}$, thus $\mathcal{C}_T(\rho) \geq \mathcal{C}_I(\rho)$ [27].

The remainder contribution for total quantum coherence is regarded as the quantum local coherence, which can be described as

$$\mathcal{C}_L(\rho) = \mathcal{D}(\delta^*, \rho^d), \quad (15)$$

where ρ^d and δ^* are obtained by minimizing Eqs. (13) and (14), respectively. In this work, we pay attention to the relative entropy $\mathcal{D}(\rho, \delta) = \text{Tr}[\rho(\log_2 \rho - \log_2 \delta)]$, which is a bona fide distance measure for quantifying both quantum coherence [3] and entanglement [26,27]. In this distance measure $\mathcal{C}_L(\rho) + \mathcal{C}_I(\rho) \geq \mathcal{C}_T(\rho)$ is satisfied.

III. RESULTS

A. Total, local, and intrinsic quantum coherence in the XY model

We study the abilities of the total, local, and intrinsic quantum coherence in characterizing the second-order QPT in the XY model. We numerically calculate the total quantum coherence of the spin-pairs ρ_{mn} , which can be decomposed of the intrinsic coherence between the m th and n th spin, and the local coherence on the m th and n th spin. The computational results of total, local, and intrinsic quantum coherence in the XY model with $\gamma = 0.6$ and 0.8 are presented in Fig. 3. From Fig. 3(a), it is shown that the intrinsic coherence $\mathcal{C}_I(\rho) = 0$ at the factorization points ($\lambda_{f1} = 0.8$ for $\gamma = 0.6$ and $\lambda_{f1} = 0.6$ for $\gamma = 0.8$). Actually, at λ_f , the reduced density operator ρ in Eq. (4) is a separable state [28,29]; thus the intrinsic coherence vanishes and the local coherence is equal to the total coherence, i.e., $\mathcal{C}_L(\rho) = \mathcal{C}_T(\rho)$, which can be observed from the inset of Fig. 3(b). Moreover, all of the total, local, and intrinsic coherence have sudden changes at the critical point of second-order QPT $\lambda_c = 1$, and the critical point can be highlighted via the coherence susceptibility with respect to λ [11], that is, $\chi(\mathcal{C}) = d\mathcal{C}/d\lambda$.

In addition, from Fig. 3(c) and 3(d), it can be observed that, although $\chi(\mathcal{C}_T)$ is trivial for factorization, $\chi(\mathcal{C}_L)$ has nonanalytical behaviors close to λ_f . In fact, Eq. (15) suggests that the local coherence is dependent on both of δ^* and ρ^d . δ^* is tightly related to the intrinsic coherence and naturally

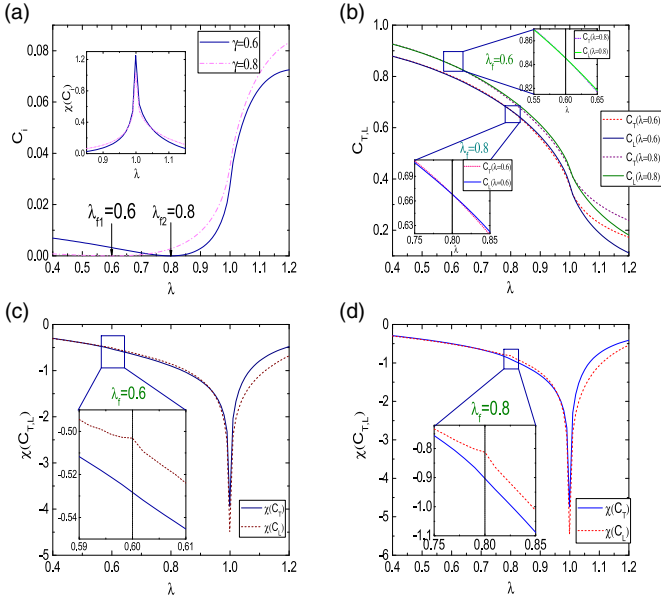


FIG. 3. (a) The intrinsic coherence C_I as functions of λ with $\gamma = 0.6, 0.8$. The inset shows the intrinsic coherence susceptibility as functions of λ with $\gamma = 0.6, 0.8$. (b) The dependence of the local and total coherence, i.e., C_L and C_T , and λ with $\gamma = 0.6, 0.8$. (c) The dependence of the local and total coherence susceptibility with respect to λ , i.e., $\chi(C_L)$ and $\chi(C_T)$, and λ with $\gamma = 0.8$. (d) The dependence of the local and total coherence susceptibility with respect to λ , i.e., $\chi(C_L)$ and $\chi(C_T)$, and λ with $\gamma = 0.6$.

contains the information of factorization. Consequently, the local coherence susceptibility can characterize the factorization phenomenon.

Furthermore, the long-range properties of the total quantum coherence are emphasized in Ref. [12,13]. With the aim to obtain relevant scaling laws, we focus on the reduced density operators for spin-pairs with long distance, i.e., $R > 1$. Without losing generalization, we only consider the XY model with $\gamma = 0.6$ here. In Fig. 4(a), the intrinsic coherence almost vanishes and $C_T \simeq C_L$ in the case of $R = 3$, indicating that the intrinsic coherence is a short-range correlation, while the total quantum coherence is a long-range correlation because the contribution from the coherence in every single qubit, that is, the local coherence, is not influenced by the increase of R . Actually, it has been revealed that although the correlation length is diverging at the critical point, the entanglement between the two sites with long distance vanishes [30], which is consistent with the results of intrinsic coherence. As shown in Fig. 4(b), the susceptibility of total quantum coherence can still detect the critical point $\lambda_c = 1$ for the spin-pairs with long distance. But the intrinsic coherence cannot characterize QPTs even with $R = 3$, see the inset of Fig. 4(a). Moreover, the impact of R on the critical behaviors of total quantum coherence is explored quantitatively. The value of total quantum coherence at critical point as a function of distance of spin-pairs R is displayed in Fig. 4(c), which reveals a power-law decay of the total quantum coherence at the critical point, i.e.,

$$C_T|_{\lambda=\lambda_c} = aR^b. \quad (16)$$

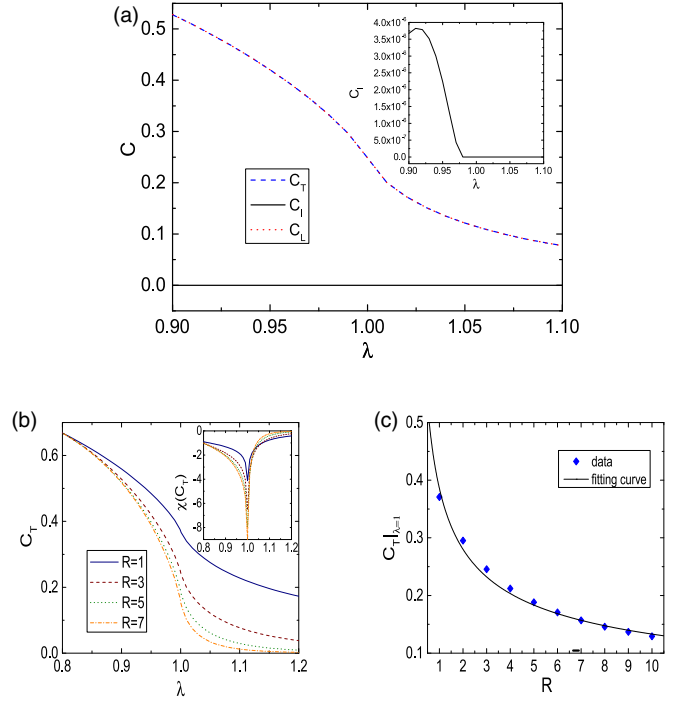


FIG. 4. (a) The intrinsic coherence, local coherence, and total coherence C_I , C_L , and C_T for the reduced density operators of spin-pairs with long distance $R = 3$ as functions of λ with $\gamma = 0.6$. (b) Total quantum coherence C_T for the reduced density operators of spin-pairs with $R = 1, 3, 5, 7$ as functions of λ . (c) The relation of the value of total quantum coherence at the critical point $\lambda_c = 1$ and distance of spin-pairs R . The expression of fitting curve is $C_T|_{\lambda=\lambda_c} = 0.3862R^{-0.4627}$.

We mention here that the polynomial scaling law of quantum discord at the critical point of the XY model has been derived analytically in Ref. [31], which shows that the quantum discord $QD(\rho_{mn}) \sim R^{-0.5}$, where $R = |m - n|$ represents the distance of spin-pairs, at $\lambda_c = 1$. In fact, quantum discord can be regarded as the quantum coherence in the particular representation obtained by minimizing over all product local unitary transformations [27]. Hence quantum coherence has the similar scaling law to quantum discord.

B. Total, local, and intrinsic quantum coherence in the extended XY model

To explore the connection between quantum coherence and TQPTs, we focus on the extended XY model, where the three-site interaction is considered. First, the total quantum coherence C_T in the extended XY model is calculated. In Figs. 5(a) and 5(c), it can be observed that C_T have pronounced local maximum behaviors at the critical points related to the TQPTs driven by the anisotropy of nearest-neighbor spins γ with parameters $\alpha = 1, \delta = 1, \lambda = -0.5$, as well as the TQPTs driven by the strength of three-site interaction α with parameters $\gamma = 1, \delta = -1, \lambda = 1$. The winding numbers as functions of γ and α are depicted in Figs. 5(b) and 5(d), respectively. The energy spectra and trajectories of winding vectors with parameters $\gamma = 1, \delta = -1, \lambda = 1$, and several values of α are presented in Appendix A carefully, which indicates

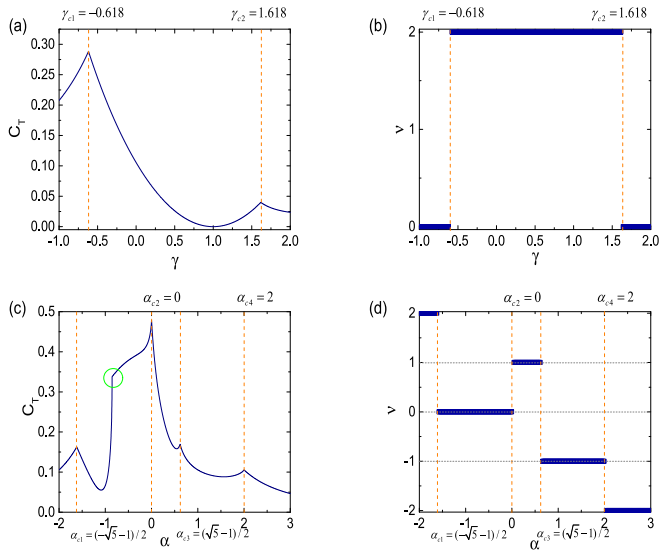


FIG. 5. Total quantum coherence as a function of γ with parameters (a) $\alpha = 1, \delta = 1, \lambda = -0.5$ and (c) as a function of α with parameters $\gamma = 1, \delta = -1, \lambda = 1$. (b) and (d) display the dependence of winding numbers on γ with the same parameters of (a) and on α with the same parameters of (c).

the locations of critical points are $\alpha_{c1} = (-\sqrt{5} - 1)/2, \alpha_{c2} = 0, \alpha_{c3} = (\sqrt{5} - 1)/2$, and $\alpha_{c4} = 2$. In contrast to the results of former works on the quantum discord [32] and the one-way deficit [33] in this model, it is intriguing that the total quantum coherence can directly spotlight the critical points related to TQPTs. However, it only can be observed that the quantum discord and the one-way deficit change dramatically around the critical points. Therefore, pinpointing the critical points requires the susceptibility of quantum discord and one-way deficit with respect to the quantities which drive TQPTs. It is noted that there is a singular point around $\alpha \simeq 0.85$, which is highlighted by the green circle in Fig. 5(c). In Appendix B, the numerical results with high accuracy are presented, which indicates that this is a discontinuity point, while at the critical points related to TQPTs, the quantum coherence behaves continuously. Thus, the singular point can not be regarded as a signature of TQPTs.

Moreover, the intrinsic coherence C_I and local coherence C_L in the extended XY model are studied. In Fig. 6(a), around the critical point $\alpha_c = 0$, the behaviors of total coherence and local coherence are similar. However, the tendency of the intrinsic coherence is different from them. For instance, the trade-off relation between intrinsic and local coherence can be observed. When $\alpha > 0.2$, both of total and local coherence decrease while intrinsic coherence increases. Most importantly, at the critical point, instead of local maximum, there is a sudden change of the intrinsic coherence and the susceptibility of intrinsic coherence $\chi(C_I) = dC_I/d\alpha$ can spotlight the critical points of TQPTs directly.

Additionally, the reduced density matrices for spin-pairs with long distance in extended XY model are considered. In Fig. 6(b), the long-range properties of the total coherence and local coherence, as well as the short-range properties of the

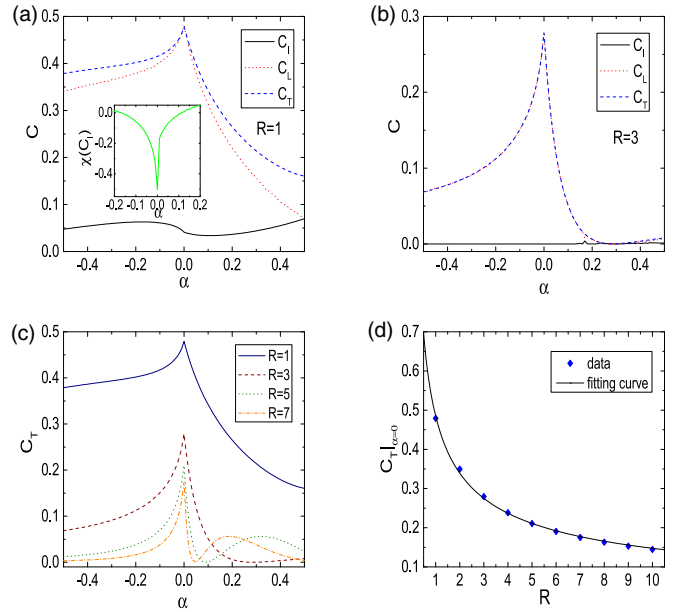


FIG. 6. (a) The total, intrinsic, and local quantum coherence as a function of α with parameters $\gamma = 1, \delta = -1, \lambda = 1$ for the reduced density operator of nearest spin-pairs, i.e., $R = 1$, and the inset shows the dependence of intrinsic quantum coherence susceptibility on α . (b) The total, intrinsic and local quantum coherence as a function of α with the same parameters in (a) except for the distance of spin-pairs $R = 3$. (c) The dependence of total quantum coherence on α with several different R . (d) The relation of the value of total quantum coherence at the critical point $\alpha_c = 0$ and distance of spin-pairs R . The expression of fitting curve is $C_T|_{\alpha=\alpha_c} = 0.4853R^{-0.5171}$.

intrinsic coherence are also observed around the critical point $\alpha_c = 0$. As displayed in Fig. 6(c), the total quantum coherence can still spotlight the critical point related to TQPT efficiently even with a long distance of spin-pairs.

Furthermore, although the total quantum coherence decays polynomially at the critical point associated with the second-order QPT in the XY model, the scaling law Eq. (16) is still worthwhile to demonstrate for TQPTs. In Fig. 6(d), the relation between total quantum coherence at the topological critical point $C_T|_{\alpha=\alpha_c}$ and R indicates that the scaling law Eq. (16) is satisfied for the critical point $\alpha_c = 0$ of TQPT.

However, as shown in Fig. 7(a), around the critical point $\alpha_c = 2$, it can be directly observed that the value of C_T with $R = 2$ is larger than $R = 1$, hence C_T does not decay monotonically with the increase of R . Then, the dependence of $C_T|_{\alpha=2}$ and R is displayed in Fig. 7(b), which indicates that the scaling law Eq. (16) is not valid for all critical points associated to TQPTs. The main difference of the TQPTs at $\alpha_c = 0$ and $\alpha_c = 2$ is that the latter is related to a topological phase with high winding number, that is $\nu = -2$. Enlightened by recent works which show that the quantum fisher information fails to characterize the topological phases with high winding numbers, while it can characterize them efficiently *in dual lattices* via scaling laws [34,35], we employ the duality transformation to explore the scaling law of total quantum coherence at $\alpha_c = 2$ (see Appendix C for details). It is noted that the duality transformation provides mathematically

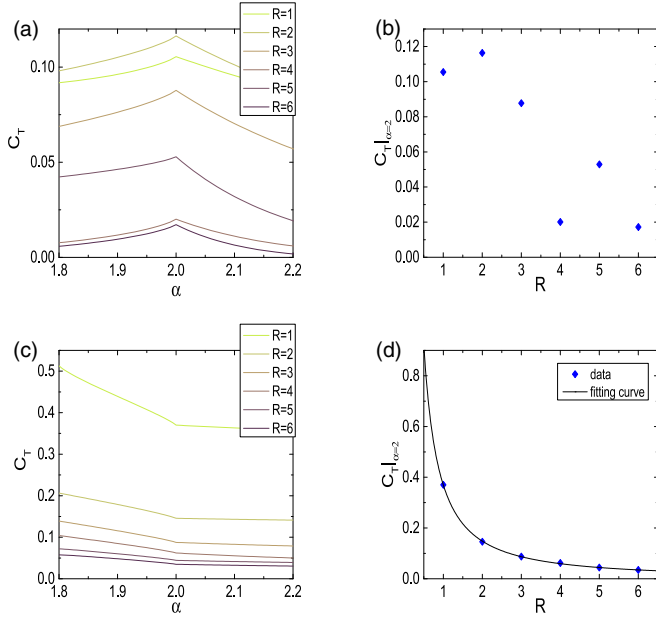


FIG. 7. (a) The total quantum coherence C_T as functions of α close to the critical point $\alpha_c = 2$ for several values of R without duality transformation. (b) The relation of $C_T|_{\alpha=2}$ and the distances of spin-pairs R without duality transformation. (c) C_T as functions of α near the critical point $\alpha_c = 2$ for several values of R in the dual lattice. (d) The relation of $C_T|_{\alpha=2}$ and the distances of spin-pairs R in the dual lattice, which can be fitted perfectly by $C_T|_{\alpha=2} = 0.3696R^{-1.371}$.

different but physically equivalent descriptions for the same physical phenomenon [36–39]. In Figs. 7(c) and 7(d), the results of C_T near $\alpha_c = 2$ in the dual lattice are presented. The critical point related to TQPT can be detected by the total quantum coherence in the dual lattice. Moreover, it is remarkable that the data of $C_T|_{\alpha=2}$ and R in the dual lattice are fitted perfectly by the scaling law Eq. (16).

C. Total, local, and intrinsic quantum coherence in the A-T model

After investigating the capabilities of total, local, and intrinsic quantum coherence in detecting the second-order QPT and TQPTs, we explore the relation of quantum coherence and infinite-order QPT. Here we study the total, local, and intrinsic quantum coherence of the frontal spin-pairs for the Ashkin-Teller (A-T) model, i.e., the reduced density operator Eq. (12).

First of all, we prove that the intrinsic coherence $C_I = 0$ for Eq. (12). The intrinsic coherence is independent of the chosen basis [9,26,27]

$$C_I(\rho_{\sigma_i-\tau_i}) = C_I(U_{\sigma_i} \otimes U_{\tau_i} \rho_{\sigma_i-\tau_i} U_{\sigma_i}^\dagger \otimes U_{\tau_i}^\dagger). \quad (17)$$

We intuitively apply the unitary transformation

$$U_{\sigma_i} = U_{\tau_i} = \frac{1}{\sqrt{2}} \begin{pmatrix} 1 & 1 \\ 1 & -1 \end{pmatrix}, \quad (18)$$

which transforms the representation from σ^z to σ^x . After that, we obtain the reduced density operator in σ^x representation,

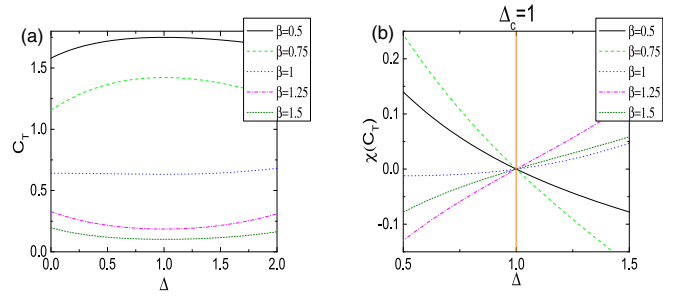


FIG. 8. The total quantum coherence C_T (a) and coherence susceptibility with respect to Δ $\chi(C_T)$ (b) as functions of Δ with various values of β .

that is

$$\begin{aligned} \rho_{\sigma_i-\tau_i}^x &= U_{\sigma_i} \otimes U_{\tau_i} \rho_{\sigma_i-\tau_i} U_{\sigma_i}^\dagger \otimes U_{\tau_i}^\dagger \\ &= \frac{1}{4} \begin{pmatrix} 2u + v + 1 & 0 & 0 & 0 \\ 0 & 1 - v & 0 & 0 \\ 0 & 0 & 1 - v & 0 \\ 0 & 0 & 0 & v - 2u + 1 \end{pmatrix}. \end{aligned} \quad (19)$$

Because $\rho_{\sigma_i-\tau_i}^x \in \mathcal{S}$ is a separable state, $C_I(\rho_{\sigma_i-\tau_i}) = C_I(\rho_{\sigma_i-\tau_i}^x) = 0$ and $C_T(\rho_{\sigma_i-\tau_i}) = C_L(\rho_{\sigma_i-\tau_i})$.

Then, the total quantum coherence in the A-T model with $N = 16$ spins is simulated numerically by performing exact diagonalization. In Fig. 8, the total quantum coherence C_T and coherence susceptibility with respect to Δ , that is, $\chi(C_T) = dC_T/d\Delta$, as functions of Δ for several values of β are displayed. It is shown that the local extreme point of C_T , which satisfies $\chi(C_T) = 0$, coincides with the critical point associated to infinite-order QPT of the A-T model. Thus, although the intrinsic coherence cannot give any signatures of the infinite-order QPT in the A-T model, the local quantum coherence, which is equal to the total coherence, can characterize the infinite-order QPT efficiently.

IV. CONCLUSION

In summary, the local, intrinsic and total quantum coherence, measured via the relative entropy in critical systems, including the XY model, extended XY model, and A-T model, are studied. All of them can pinpoint the critical point associated with the second-order QPT in the XY model. It is intriguing that the local coherence have nontrivial at the factorization point. However, the total coherence is anesthetic to factorization. Moreover, the nonanalytical behaviors of total coherence and local coherence can directly spotlight the critical points related to TQPTs in the extended XY model. Whereas, instead of local maximum, a significant change of the intrinsic coherence can be observed around the critical points. In addition, for the frontal spin-pairs of the A-T model, intrinsic coherence is proven to be zero and the local coherence is equal to the total coherence. The extreme points of the total coherence can characterize the infinite-order QPT in the A-T model.

Furthermore, the critical behaviors of quantum coherence for the spin-pairs with long distance of the XY model and

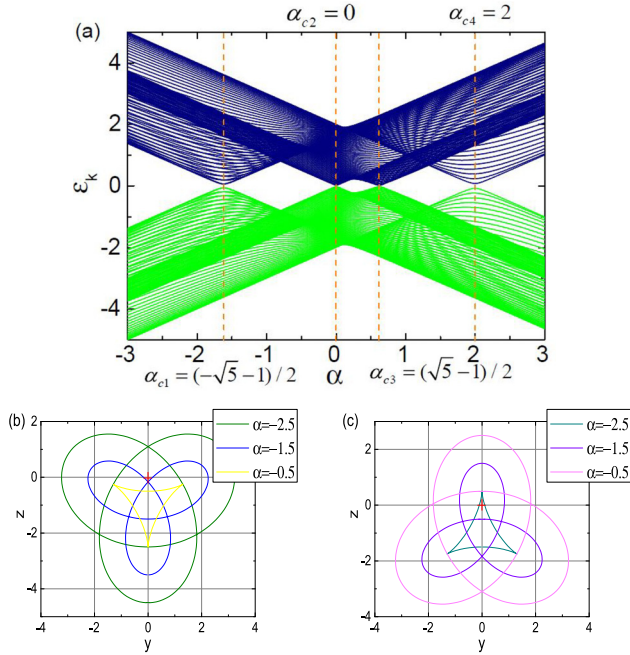


FIG. 9. (a) The energy spectra as a function of α with parameters $\gamma = 1$, $\delta = -1$, $\lambda = 1$. (b, c) Trajectories of winding vectors in Y - Z plane for parameters $\gamma = 1$, $\delta = -1$, $\lambda = 1$ with various values of α . For $\alpha = -2.5, -1.5, -0.5, 0.5, 1.5, 2.5$, the winding numbers are $\nu = 2, 0, 0, 1, -1, -2$, respectively.

extended XY model are investigated. It is shown that the long-range properties of total quantum coherence are originated from the local coherence, while the intrinsic coherence is regarded as a short-range correlation. Additionally, the connection between the distance of spin-pairs and the value of total coherence at a critical point reveals the power-law decay of the total quantum coherence at critical points related to the second-order QPTs in the XY model as well as the TQPTs in the extended XY model. It is noted that the power-law decay of total coherence can only be observed in the dual lattices in the case of the TQPTs are related to topological phases with high winding numbers.

The results of this work suggest that not only the total quantum coherence, but also the local and intrinsic quantum coherence can recover rich physics in condensed-matter systems and are worthwhile to explore for other critical systems, such as spin-1 chains [40] and transverse-field XXZ model [41], as well as the quantum optics systems with the QPTs between the normal phase and the superradiant phase, for instance, the quantum Rabi model [42,43] and the Dicke model [44]. Although the computation of intrinsic quantum coherence is a heavy numerical task [45], with the rapid developments of calculation methods for multipartite entanglement [46,47], the properties of local and intrinsic quantum coherence in the above systems will be investigated.

ACKNOWLEDGMENTS

We are thankful to Dr. Chandrashekar Radhakrishnan, Professor Tim Byrnes, Dr. Yu-Ran Zhang, and Professor Heng Fan for communications.

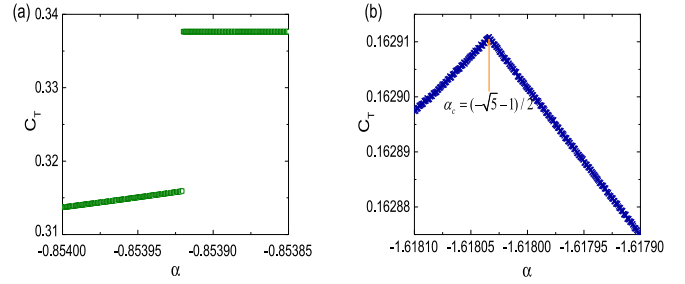


FIG. 10. The dependence of total quantum coherence C_T and α around (a) $\alpha = -0.85$ and (b) $\alpha = (-\sqrt{5} - 1)/2$.

APPENDIX A: GROUND-STATE ENERGY SPECTRUM AND TRAJECTORIES OF WINDING VECTORS FOR THE PARAMETERS $\gamma = 1$, $\delta = -1$, $\lambda = 1$ WITH DIFFERENT α IN THE EXTENDED XY MODEL

In Appendix A, we give the calculation results of the energy spectra and trajectories of winding vectors with parameter $\gamma = 1$, $\delta = -1$, $\lambda = 1$ for various values of α . In this case, the characteristic function is $g(\xi) = \alpha\xi^2 + \frac{1}{\xi} - 1 = 0$ with $\xi = \exp(ik)$ and $|\xi| = 1$. The critical points associated with TQPTs are $\alpha_{c1} = (-\sqrt{5} - 1)/2$, $\alpha_{c2} = 0$, $\alpha_{c3} = (\sqrt{5} - 1)/2$, and $\alpha_{c4} = 2$ with $\xi_1 = \exp\{\pm \arccos[(1 - \sqrt{5})/4]\}$, $\xi_2 = 1$, $\xi_3 = \exp\{\pm \arccos[(1 + \sqrt{5})/4]\}$, and $\xi_4 = -1$, respectively. The location of critical points can also be highlighted from the energy spectrum as shown in Fig. 9(a). In addition, from the trajectories of the winding vectors in the Y - Z plane displayed in Figs. 9(b) and 9(c), the winding number as a function of α , that is, the Fig. 5(d) in the main text, can be directly obtained.

APPENDIX B: NUMERICAL RESULTS WITH HIGH ACCURACY AROUND $\alpha = -0.85$ AND $\alpha = (-\sqrt{5} - 1)/2$

In this Appendix, we present the numerical results of total quantum coherence C_T with high accuracy around $\alpha = -0.85$ and $\alpha = 0$. The parameters are set as $\gamma = 1$, $\delta = -1$, and $\lambda = 1$. At $\alpha = (-\sqrt{5} - 1)/2$, the TQPT occurs. In Fig. 10(a), we can observe the discontinuity of C_T around $\alpha = -0.85$. However, at the critical points associated with TQPTs, the C_T is continuous. Therefore, the singular behavior of C_T around $\alpha = -0.85$ cannot be regarded as a signature of TQPT.

APPENDIX C: DUALITY TRANSFORMATION

In this Appendix, we present the details of the duality transformation. Since the critical point $\alpha_c = 2$ is related to the topological phase with winding number $\nu = -2$, we employ the duality transformation

$$\mathbb{Z}_n = \sigma_n^y \sigma_{n+1}^y, \quad (C1)$$

$$\mathbb{Y}_n = \prod_{l=1}^n \sigma_l^z, \quad (C2)$$

$$\mathbb{X}_n = - \left(\prod_{l=1}^{n-1} \sigma_l^z \right) \sigma_n^x \sigma_{n+1}^y. \quad (C3)$$

In the dual lattice, the reduced density operators for the spin-pairs ρ_{mn} can be written as

$$\rho_{mn} = \frac{1}{4} \begin{pmatrix} w^+ & 0 & 0 & v^- \\ 0 & z & v^+ & 0 \\ 0 & v^+ & z & 0 \\ v^- & 0 & 0 & w^- \end{pmatrix}, \quad (\text{C4})$$

where $w^\pm = 1 \pm (\langle \mathbb{Z}_m \rangle + \langle \mathbb{Z}_n \rangle) + \langle \mathbb{Z}_m \mathbb{Z}_n \rangle$, $z = 1 - \langle \mathbb{Z}_m \mathbb{Z}_n \rangle$, and $v^\pm = \langle \mathbb{X}_m \mathbb{X}_n \rangle \pm \langle \mathbb{Y}_m \mathbb{Y}_n \rangle$.

The correlation functions in the dual lattice read

$$\langle \mathbb{Z}_m \rangle = \langle \sigma_m^y \sigma_{m+1}^y \rangle, \quad (\text{C5})$$

$$\langle \mathbb{Z}_m \mathbb{Z}_n \rangle = \langle \sigma_m^y \sigma_{m+1}^y \sigma_n^y \sigma_{n+1}^y \rangle, \quad (\text{C6})$$

$$\begin{aligned} \langle \mathbb{Y}_m \mathbb{Y}_n \rangle &= \left\langle \prod_{l=1}^m (\sigma_l^z) \prod_{j=1}^n (\sigma_j^z) \right\rangle \\ &= \langle \sigma_{m+1}^z \sigma_{m+2}^z \cdots \sigma_n^z \rangle, \end{aligned} \quad (\text{C7})$$

$$\langle \mathbb{X}_m \mathbb{X}_n \rangle = \left\langle \prod_{l=m}^{n-1} (\sigma_l^y \sigma_{l+1}^z \sigma_{l+2}^y) \right\rangle, \quad (\text{C8})$$

which can be calculated by applying the Wick theorem and the transformation

$$\sigma_n^x = A_n \prod_{l=1}^{n-1} A_l B_l, \quad (\text{C9})$$

$$\sigma_n^y = -i B_n \prod_{l=1}^{n-1} A_l B_l, \quad (\text{C10})$$

$$\sigma_n^z = -A_n B_n, \quad (\text{C11})$$

The operators A_n and B_m satisfy

$$\langle A_m A_n \rangle = \delta_{mn}, \quad \langle B_m B_n \rangle = -\delta_{mn}, \quad (\text{C12})$$

and

$$\langle A_m B_n \rangle = G_R = -\frac{1}{\pi} \int_0^\pi dk \cos(Rk - \theta_k), \quad (\text{C13})$$

where $R = |m - n|$ and θ_k is given in the Eq. (3) of the main text.

For instance, in the case of $R = 2$,

$$\langle \mathbb{Z}_m \rangle = \langle \mathbb{Z}_n \rangle = G_1, \quad (\text{C14})$$

$$\begin{aligned} \langle \mathbb{X}_m \mathbb{X}_{m+2} \rangle &= \langle A_m B_{m+2} A_{m+1} B_{m+3} \rangle \\ &= G_2^2 - G_3 G_1, \end{aligned} \quad (\text{C15})$$

$$\begin{aligned} \langle \mathbb{Y}_m \mathbb{Y}_{m+2} \rangle &= \langle A_m B_m A_{m+1} B_{m+1} \rangle \\ &= G_0^2 - G_1 G_{-1}, \end{aligned} \quad (\text{C16})$$

$$\begin{aligned} \langle \mathbb{Z}_m \mathbb{Z}_{m+2} \rangle &= \langle A_m B_{m+1} A_{m+2} B_{m+3} \rangle \\ &= G_1^2 - G_3 G_{-1}. \end{aligned} \quad (\text{C17})$$

-
- [1] A. Streltsov, G. Adesso, and M. B. Plenio, *Rev. Mod. Phys.* **89**, 041003 (2017).
- [2] M.-L. Hu, X. Hu, J.-C. Wang, Y. Peng, Y.-R. Zhang, and H. Fan, [arXiv:1703.01852](https://arxiv.org/abs/1703.01852).
- [3] T. Baumgratz, M. Cramer, and M. B. Plenio, *Phys. Rev. Lett.* **113**, 140401 (2014).
- [4] A. E. Rastegin, *Phys. Rev. A* **93**, 032136 (2016).
- [5] S. Rana, P. Parashar, and M. Lewenstein, *Phys. Rev. A* **93**, 012110 (2016).
- [6] L.-H. Shao, Z. Xi, H. Fan, and Y. Li, *Phys. Rev. A* **91**, 042120 (2015).
- [7] D. Girolami, *Phys. Rev. Lett.* **113**, 170401 (2014).
- [8] C. S. Yu, *Phys. Rev. A* **95**, 042337 (2017).
- [9] C. Radhakrishnan, M. Parthasarathy, S. Jambulingam, and T. Byrnes, *Phys. Rev. Lett.* **116**, 150504 (2016).
- [10] S. Sachdev, *Quantum Phase Transition* (Cambridge University Press, Cambridge, England, 1999).
- [11] J.-J. Chen, J. Cui, Y.-R. Zhang, and H. Fan, *Phys. Rev. A* **94**, 022112 (2016).
- [12] C. Radhakrishnan, I. Ermakov, and T. Byrnes, *Phys. Rev. A* **96**, 012341 (2017).
- [13] Y.-T. Sha, Y. Wang, Z.-H. Sun, and X.-W. Hou, *Ann. Phys.* **392**, 229 (2018).
- [14] G. Karpat, B. Çakmak, and F. F. Fanchini, *Phys. Rev. B* **90**, 104431 (2014).
- [15] X. G. Wen, *Quantum Field Theory of Many-Body Systems* (Oxford University Press, New York, 2004).
- [16] X. Y. Feng, G. M. Zhang, and T. Xiang, *Phys. Rev. Lett.* **98**, 087204 (2007).
- [17] G. Zhang and Z. Song, *Phys. Rev. Lett.* **115**, 177204 (2015).
- [18] J. Ashkin and E. Teller, *Phys. Rev.* **64**, 178 (1943).
- [19] P. Bak, P. Kleban, W. N. Unertl, J. Ochab, G. Akinci, N. C. Bartelt, and T. L. Einstein, *Phys. Rev. Lett.* **54**, 1539 (1985).
- [20] C. C. Rulli and M. S. Sarandy, *Phys. Rev. A* **81**, 032334 (2010).
- [21] C. C. Rulli and M. S. Sarandy, *Phys. Rev. A* **84**, 042109 (2011).
- [22] E. Lieb, T. Schultz, and D. Mattis, *Ann. Phys. (N. Y.)* **16**, 407 (1961).
- [23] E. Barouch and B. M. McCoy, *Phys. Rev. A* **2**, 1075 (1970).
- [24] E. Barouch and B. M. McCoy, *Phys. Rev. A* **3**, 786 (1971).
- [25] S. Campbell, J. Richens, N. L. Gullo, and T. Busch, *Phys. Rev. A* **88**, 062305 (2013).
- [26] V. Vedral and M. B. Plenio, *Phys. Rev. A* **57**, 1619 (1998).
- [27] Y. Yao, X. Xiao, L. Ge, and C. P. Sun, *Phys. Rev. A* **92**, 022112 (2015).
- [28] S. M. Giampaolo, G. Adesso, and F. Illuminati, *Phys. Rev. Lett.* **104**, 207202 (2010).
- [29] S. M. Giampaolo, G. Adesso, and F. Illuminati, *Phys. Rev. Lett.* **100**, 197201 (2008).
- [30] A. Osterloh, L. Amico, G. Falci, and R. Fazio, *Nature* **416**, 608 (2002).
- [31] Y. Huang, *Phys. Rev. B* **89**, 054410 (2014).
- [32] X. Z. Zhang and J. L. Guo, *Quant. Inf. Proc.* **16**, 223 (2017).
- [33] Y.-K. Wang, Y.-R. Zhang, and H. Fan, [arXiv:1701.01629](https://arxiv.org/abs/1701.01629).

- [34] Y.-R. Zhang, Y. Zeng, H. Fan, J. Q. You, and F. Nori, *Phys. Rev. Lett.* **120**, 250501 (2018).
- [35] L. Pezzè, M. Gabbriellini, L. Lepori, and A. Smerzi, *Phys. Rev. Lett.* **119**, 250401 (2017).
- [36] S. Suzuki, J.-I. Inoue, and B. K. Chakrabarti, *Quantum Ising Phases and Transitions in Transverse Ising Models*, Vol. 862, (Springer, New York, 2012).
- [37] E. Cobanera, G. Ortiz, and Z. Nussinov, *Adv. Phys.* **60**, 679 (2011).
- [38] Y. Q. Qin, Y. Y. He, Y. Z. You, Z. Y. Lu, A. Sen, A. W. Sandvik, C. K. Xu, and Z. Y. Meng, *Phys. Rev. X* **7**, 031052 (2017).
- [39] P. Smacchia, L. Amico, P. Facchi, R. Fazio, G. Florio, S. Pascazio, and V. Vedral, *Phys. Rev. A* **84**, 022304 (2011).
- [40] A. L. Malvezzi, G. Karpat, B. Çakmak, F. F. Fanchini, T. Debarba, and R. O. Vianna, *Phys. Rev. B* **93**, 184428 (2016).
- [41] S. Mahdavifar, S. Mahdavifar, and R. Jafari, *Phys. Rev. A* **96**, 052303 (2017).
- [42] M.-J. Hwang, R. Puebla, and M. B. Plenio, *Phys. Rev. Lett.* **115**, 180404 (2015).
- [43] B.-B. Wei and X.-C. Lv, *Phys. Rev. A* **97**, 013845 (2018).
- [44] C. Emary and T. Brandes, *Phys. Rev. E* **67**, 066203 (2003).
- [45] O. Gühne and G. Tóth, *Phys. Rep.* **474**, 1 (2009).
- [46] J. Shang and O. Gühne, *Phys. Rev. Lett.* **120**, 050506 (2018).
- [47] T. Kraft, C. Ritz, N. Brunner, M. Huber, and O. Gühne, *Phys. Rev. Lett.* **120**, 060502 (2018).